Muscle Network of Parkinson's Gait: A 12-Month Longitudinal Analysis Before and After Deep Brain Stimulation Surgery

Muscle Network of Parkinson's Gait: A 12-Month Longitudinal Analysis Before and After Deep Brain Stimulation Surgery

Marco Ghislieri, Lorenzo Locoratolo, Fabrizio Sciscenti, Michele Lanotte, Laura Rizzi, and Valentina Agostini

***Abstract*— Bilateral Deep Brain Stimulation (DBS) of the subthalamic nucleus is commonly used for treating motor symptoms in patients with advanced Parkinson's Disease (PD). The aim of this study is to quantitatively and non-invasively evaluate motor control changes in PD patients following DBS through an approach based on the combination of graph theory and frequency-domain electromyography (EMG) analysis. Instrumented gait analysis was carried out on a group of 30 PD patients and 30 age-matched controls. PD patients were longitudinally followed up, with assessments pre-DBS implant (T_0), 3 months post-DBS implant (T_1), and 12 months post-DBS implant (T_2). EMG signals from 12 lower-limb and trunk muscles were acquired, calculating Inter-Muscular Coherence (IMC) for each muscle pair. Adjacency matrices derived from IMC were used to generate 3D muscle networks through a force-based algorithm. Two families of network parameters were extracted: global metrics (modularity and density) and local metrics (node strength and local clustering coefficient). Muscle network modularity of PD patients at T_0 was significantly lower than that of controls (0.34 ± 0.07 vs. 0.41 ± 0.07; $p = 0.003$) and this difference persisted at T1 (0.35 ± 0.01; $p = 0.037$), but not at T2 (0.38 ± 0.01; $p = 1.00$). Analogously, muscle network density was higher in PD patients at T_0 (T0: 0.69 ± 0.10 vs. Controls: 0.56 ± 0.10; $p = 0.004$), decreased at T_1 (0.65 ± 0.14; $p = 0.034$), and was comparable to that of controls at T_2 (0.60 ± 0.14; $p = 1.00$). Node-level analyses similarly showed that PD patients values moved toward control-group reference levels after DBS surgery, reflecting reduced individual muscle connectivity and a more structured pattern of muscle coordination. Global metrics showed a good agreement with respect to the clinical score UPDRS-III. Graph theory applied to EMG analysis opens new perspectives in the study of motor control strategies during gait and confirms the efficacy of DBS in alleviating motor symptoms of PD patients.**

***Index Terms*— EMG, intermuscular coherence, locomotion, muscle coordination, DBS.**

I. Introduction

PARKINSON'S Disease (PD) is a chronic neurodegenerative disorder primarily characterized by a reduction in dopamine synthesis within the substantia nigra pars compacta [1]. This dopaminergic impairment manifests in several cardinal motor symptoms, including akinesia, bradykinesia, hypokinesia, postural instability, and rigidity [2]. Additionally, patients with PD may experience episodic disturbances in gait, such as Freezing of Gait (FoG) or festination [3], [4].

The primary medical treatment for PD over the years has predominantly involved the chronic administration of dopaminergic agents, such as levodopa (L-dopa), which act by enhancing dopaminergic transmission [5], [6]. However, in clinical cases where pharmacological treatments have limited efficacy, electroceutical techniques such as Deep Brain Stimulation (DBS) of the SubThalamic Nucleus (STN) proved to be a valid therapeutical alternative [7]. Since the first cases of advanced PD treated with high-frequency STN-DBS, significant improvements in PD motor symptoms, including tremor, rigidity, and bradykinesia were reported. To date, thousands of patients worldwide have undergone STN-DBS implant neurosurgery, demonstrating substantial symptomatic relief, thereby establishing this technique as the standard surgical intervention for advanced PD [8].

Gait disturbances are a prominent feature of PD, increasingly contributing to disability as the disease progresses [9]. However, the detection of subtle gait alterations using the Unified Parkinson's Disease Rating Scale (UPDRS) Part III (i.e., motor examination) remains limited [10]. Consequently, the need for an objective functional evaluation to assess the efficacy of DBS in PD patients is of the utmost importance [11].

A more comprehensive understanding of the functional deficits within the impaired nervous system of PD patients may be achieved by recording and analyzing the activity of the primary muscles involved in locomotion using surface

Received 24 September 2025; revised 12 February 2026; accepted 5 April 2026. Date of publication 9 April 2026; date of current version 20 April 2026. Associate Editor: Ming Liu. This work was supported by the PD–DBS Project (Effect of bilateral subthalamic nucleus deep brain stimulation on gait analysis and muscle synergy patterns of patients affected by Parkinson's Disease during dual-task walking)—funded by European Union—Next Generation European Union (EU) within the Progetti di Rilevante Interesse Nazionale (PRIN) 2022 Program (D.D. 104—2 February 2022 Ministero dell'Università e della Ricerca) under Grant 2022KWSJJT. This manuscript reflects only the authors' views and opinions, and the ministry cannot be considered responsible for them. *(Corresponding author: Marco Ghislieri).*

This work involved human subjects. Approval of all ethical and experimental procedures and protocols was granted by the Ethics Committee of A. O. U. Cittàdella Salute e della Scienza di Torino—A. O. Ordine Mauriziano—A. S. L. "Cittàdi Torino" under Application No. 0092029, September 11, 2018.

Marco Ghislieri, Lorenzo Locoratolo, Fabrizio Sciscenti, and Valentina Agostini are with the Department of Electronics and Telecommunications and the Polito^{BIO}Med Lab, Politecnico di Torino, 10129 Turin, Italy (e-mail: marco.ghislieri@polito.it; lorenzo.locoratolo@polito.it; fabrizio.sciscenti@polito.it; valentina.agostini@polito.it).

Michele Lanotte and Laura Rizzi are with the Department of Neuroscience "Rita Levi Montalcini," University of Turin, 10126 Turin, Italy (e-mail: michele.lanotte@unito.it; l.rizzi@unito.it).

This article has supplementary downloadable material available at https://doi.org/10.1109/TNSRE.2026.3682388, provided by the authors.

Digital Object Identifier 10.1109/TNSRE.2026.3682388

electromyography (EMG) [12]. The insights gained from EMG analysis regarding the dynamic contractile activity of muscles during both healthy and pathological movements can offer valuable information [13], [14], [15]. This information can aid in various clinical tasks, including supporting the diagnosis of PD [16], characterizing hallmark motor symptoms of the disease [17], [18], and evaluating therapeutic interventions, such as assessing the impact of levodopa or high-frequency DBS on muscle activation patterns and synergies in PD patients [19], [20], [21].

The muscle synergy theory posits that the Central Nervous System (CNS) manages the activation levels and synchrony of muscles involved in specific motor tasks through a limited set of low-dimensional elements, referred to as muscle synergies, rather than exerting independent control over each individual muscle [22]. Despite this, the mechanisms by which the CNS reduces the numerous degrees of freedom within the musculoskeletal system remain inadequately understood, posing a significant challenge. Consequently, novel methodologies have been developed to assess coordination during gait and postural tasks. Among these methodologies, the integration of network theory with EMG signal analysis has produced promising findings, particularly in the context of postural tasks [23], [24] and walking [25]. Complex network analysis, a technique widely utilized to characterize the organization of distributed brain activity, has demonstrated that brain networks exhibit many features common to other complex physical and biological systems [26]. The muscle networks approach, rooted in graph theory, quantifies the topological structures of these systems by analyzing their respective network representation [27], [28].

Graph theory, a branch of mathematics, examines the properties and applications of graphs - graphical representations used to model pairwise relationships between objects. This framework is applicable across diverse fields, including computer science, biology, and social sciences. Graphs can be classified as directed or undirected, depending on whether the connections between nodes possess a specific direction, and as weighted or unweighted, depending on whether the connections carry associated values or costs. An undirected weighted graph is typically made up of nodes (in our case, muscles) that are connected by edges (also called links or lines) that connect the nodes with a specific weight, i.e., the stronger the link between nodes, the higher the edge's weight. Force-directed algorithms are among the most versatile methods for calculating layouts of simple undirected graphs. Graphs generated through these algorithms tend to be aesthetically pleasing and clear, often producing layouts that are intersection-free and exhibit high levels of symmetry [29].

In this study, we intend to generate muscle network graphs based on the calculation of Inter-Muscular Coherence (IMC). IMC is a widely utilized method for investigating motor control characteristics [30] and it refers to the analysis of linear dependencies between two EMG recordings at specific frequencies [31]. It is computed between pairs of EMG signals originating from different muscles or within different regions of the same muscle, the latter referred to as intramuscular coherence [32], [33], [34]. Coherence between two signals can be conceptualized as the frequency-domain counterpart of (time-domain) Pearson's correlation used to quantify synchrony in time series. IMC is associated with both cortical and spinal mechanisms [35], [36] and serves as a tool for evaluating the synchronization of neural inputs across different muscles. Unlike time-domain correlation methods, coherence allows for quantification of the entire frequency spectrum of synchronization between EMG signals [37]. Consequently, IMC is particularly valuable in the study of motor control and neurophysiological processes, as evidenced by its extensive application in numerous studies [38], [39], [40].

This integrative approach was adopted to simultaneously assess distinct aspects of motor control. Intermuscular coherence defines physiologically grounded functional connections, network theory formalizes these connections into analyzable structures that capture system-level organization, and force-based graph layouts provide an interpretable visualization that supports both qualitative interpretation and quantitative analysis.

To the best of the authors' knowledge, there are currently no studies integrating the concepts of intermuscular coherence and muscle network graphs to assess the functional coordination of PD patients during locomotion before and after STN-DBS neurosurgery. The aim of this work is to explore the potentialities of graph theory for the evaluation of PD gait coordination before and after DBS, by building a force-directed, weighted network of the muscles mainly involved in locomotion. To this purpose, an experimental population of 30 PD patients was assessed during EMG-based gait analysis at three time points: (*i*) before DBS implant (baseline, T_0), (*ii*) 3 months after DBS implant (T_1), and (*iii*) 12 months after DBS implant (T_2). An age-matched population of 30 healthy subjects was used as a reference group. We hypothesize that specific graph-derived metrics (i.e., graph modularity and density) extracted from the muscle networks can provide direct measurements of the overall motor performance and gait coordination, able to objectively quantify the motor changes in PD patients after DBS implant. Specifically, we expect PD patients at baseline to show higher network density and lower modularity than healthy controls, reflecting a less refined and simplified motor control strategy with widespread muscle co-contractions. After DBS, we expect a progressive decrease in network density and a concomitant increase in modularity across follow-up time points, approaching the values observed in healthy controls. A similar temporal evolution is also expected for the local metrics (node strength and local clustering coefficients). These novel digital biomarkers - calculated from inter-muscular (EMG-EMG) coherence - can provide new knowledge on the complex mechanisms behind physiological and pathological motor control during gait and can be used both to longitudinally assess a single PD patient and to evaluate the overall improvements of a PD population after DBS. The concordance analysis between the newly proposed graph metrics and the clinical motor scale UPDRS-III was also included in the present study.

II. Materials and Methods

A. Sample Populations

A total of 60 volunteers, 30 patients with PD and 30 age-matched non-Parkinsonian controls, were enrolled in this study. Patients with PD were recruited at the Stereotactic and Functional Neurosurgery Unit of the University of

Turin (Turin, Italy) among those eligible for bilateral high-frequency DBS surgery. A reference population of healthy control subjects was recruited among patients' caregivers (i.e., wives/husbands or partners). The sample size was determined a priori using G*Power 3.1 [41] with $\alpha = 0.05$, power = 0.80, and an expected effect size of 0.80, obtaining a minimum of 26 participants per group. This sample size is also consistent with previous studies investigating locomotor control in PD patients before and after DBS [12], [42].

The PD patients were included in the study if they received a diagnosis of PD according to the UK Brain Bank principles, if they were under the age of 70, if they showed a good levodopa response according to the Levodopa Challenge Test (LSC), if they showed dyskinesia and treatment-resistant motor fluctuations, and if they were able to walk independently for at least 5 minutes, during their best-ON time window, without walking aids or external support. Exclusion criteria were: dementia or severe cognitive impairment, psychiatric or behavioral disturbances, freezing of gait and postural instability unresponsive to pharmacological treatment, brain MRI abnormalities or relevant condition that could increase surgical risk, major orthopedic conditions (e.g., hip or knee prosthesis), or co-morbidities that could alter gait patterns. The subjects in the control group were also excluded in case of musculoskeletal or neurological disorders affecting locomotion. Furthermore, both PD and healthy volunteers underwent neuropsychological and behavioral assessments through the Mini-Mental State Examination (MMSE) [43] for evaluating the global cognitive function, and the Frontal Assessment Battery (FAB) [44]. Only subjects achieving MMSE≥ 25 (i.e., normal cognitive function) and FAB≥ 15.3 were included.

This study was approved by the Ethics Committee of A.O.U. Città della Salute e della Scienza di Torino–A.O. Ordine Mauriziano–A.S.L. "Città di Torino" (No. 0092029, September 11, 2018). Following the Declaration of Helsinki, all participants provided written informed consent for the experimental procedure.

B. Experimental Protocol and Data Acquisitions

The subject preparation and sensor placement required approximately 20 minutes per subject. The bipolar active probes of the STEP32 system (Medical Technology, Turin, Italy) were positioned as represented in **Figure 1A**. The inter-electrode distance of the EMG probes was 12 mm. The sampling frequency was 2 kHz. By placing foot-switch sensors (FSW) under the heel and the 1st and 5th metatarsal heads of each foot, gait events (also sampled at 2 kHz) were tracked throughout the gait analysis session, synchronized with EMG signals.

Surface EMG signals were recorded during gait, from the following 12 muscles: left and right Longissimus Dorsii (LD), Tensor Fasciae Latae (TFL), Gluteus Medius (GMD), Rectus Femoris (RF), Lateral Hamstring (LH), Medial Hamstrings (MH), Vastus Medialis (VM), Lateral Gastrocnemius (LGS), Peroneus Longus (PL), Soleus (SOL), and Tibialis Anterior (TA). For PD patients, the most affected lower limb (identified by clinicians as the side where Parkinson's disease symptoms first appeared) was instrumented. These muscles were selected to represent the main muscle groups controlling the hip, knee, and ankle joints during gait and to include a trunk muscle pair to assess frontal-plane trunk control, which is often impaired in PD. For 13 patients, the most affected lower limb was the right (and for 17 patients it was the left). For controls, the dominant lower limb (identified as the leg used to kick the ball) was instrumented (2 left and 28 right sides).

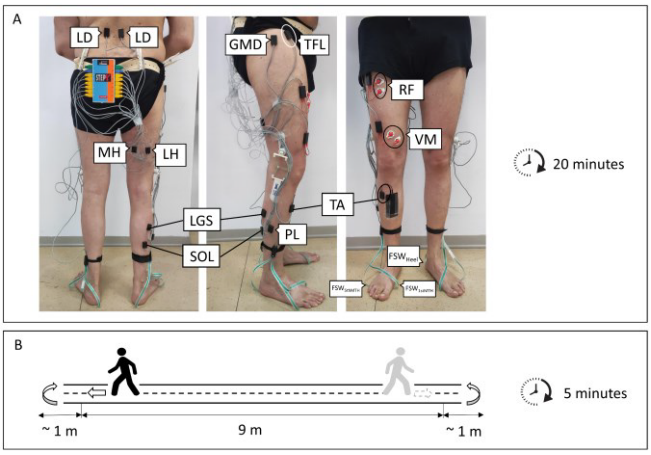

Fig. 1. Experimental setup and walking protocol. (A) Placement of electromyography (EMG) probes and foot-switches (FSW) on a representative Parkinson's Disease (PD) patient. Surface EMG sensors are positioned over 12 muscles relevant for gait analysis (listed in proximal to distal order): left and right Longissimus Dorsii (LD), Tensor Fasciae Latae (TFL), Gluteus Medius (GMD), Rectus Femoris (RF), Lateral Hamstring (LH), Medial Hamstrings (MH), Vastus Medialis (VM), Lateral Gastrocnemius (LGS), Peroneus Longus (PL), Soleus (SOL), and Tibialis Anterior (TA). Notice that the right lower limb is instrumented in this case, since it is the most-affected side of this specific patient. Foot-switches are placed under the heel (FSW_{Heel}), the first ($FSW_{1\ stMTH}$), and the fifth ($FSW_{5\ thMTH}$) metetarsal heads to detect gait events. The subject preparation lasts approximately 20 minutes. (B) Schematic representation of the walking path. The subject is asked to walk for 5 minutes (at self-selected pace), back and forth a 9-m straight path.

After mounting the EMG probes and foot-switches on the subject, the instrumented gait analysis session started. The subject was asked to walk for 5 minutes - at a self-selected pace - back and forth a 9-m straight walkway (see **Figure 1B**). PD patients were tested three times: at baseline (before DBS, T_0), at 3 months (T_1), and at 12 months (T_2) after the DBS implant. During the follow-up, the DBS parameters were tailored to the PD patients' needs to obtain the best possible clinical outcome. In particular, the T_1 and T_2 experimental sessions were conducted during best-ON conditions (i.e., best pharmacological time window and optimal DBS programming settings as defined by the treating neurologists). At T_0 and T_2, PD patients were also clinically assessed by treating clinicians using the Hoehn and Yahr (H&Y) scale and Unified Parkinson's Disease Rating Scale (UPDRS) Part III [45], [46]. Healthy controls performed the gait analysis only once. All the gait analysis sessions were carried out at the Motion Analysis Laboratory of the PolitoBIOMed Lab (Politecnico di Torino, Turin, Italy).

The EMG and foot-switch signals acquired were processed (offline) through custom routines written in MATLAB, release R2024a (MathWorks Inc., Natick, MA, USA), as described in the following section.

C. Pipeline for Muscle-Network Graph Extraction

First, EMG signals were pre-processed and, then, a muscle-network graph of each subject was extracted using the pipeline schematized in **Figure 2**, as described below.

1) **EMG pre-processing:** for each EMG signal, the following pre-processing procedure was applied:

a) *Detection of the epoch of interest:* starting from a continuous walking trial of 5 minutes along a 9-m walkway, we excluded signal epochs related to gait initiation, gait termination, direction changes at the beginning and end of the walkway, brief pauses, etc., focusing our analysis of muscle coordination on walking bouts related to steady-state walking (at self-selected speed) along straight-path segments;

b) *EMG filtering:* EMG signals were band-pass filtered (8^{th}-order zero-lag Butterworth digital filter) between 20 and 400 Hz. The lower cutoff frequency was set at 20 Hz to remove motion artifacts [47]. In PD patients' post-surgery (at T_1 and T_2), the EMG signals from dorsal muscles and other proximal muscles were often affected by DBS stimulation artifacts at the stimulation frequency (and its harmonics) [48]. Therefore, for those muscles in which the Power Spectral Density (PSD) of the EMG signal showed peaks related to the presence of DBS stimulation artifacts (i.e., at 130 Hz, 260 Hz, etc.), a recursive notch filter (8^{th} order, quality factor = 25) was applied at the stimulation frequency and its harmonics.

To avoid power spectrum distortion of EMG signals [49], [50], [51], [52], no full-wave rectification was performed prior to muscle network extraction. An example of filtered EMG signals of a representative subject is shown in **Figure 2A** (only an epoch of 5 s is displayed).

2) **Muscle network extraction:** for each subject (and each time point in the case of PD patients), a muscle network was extracted by adopting the following procedure:

a) *Inter-Muscular Coherence (IMC):* Inter-Muscular Coherence (IMC), also named EMG-EMG coherence, was calculated between each pair of muscles (i, j, with $i \neq j$) defined as in **Equation (1)**:

$$C_{i,j}(f) = \frac{|S_{i,j}(f)|^2}{S_{i,i}(f) \cdot S_{j,j}(f)} \quad (1)$$

where $S_{i,j}$ is the Cross-Spectral Density (CSD) and $S_{i,i}$ and $S_{j,j}$ are the Power auto-Spectral Densities (PSDs) of EMG signals recorded from the two muscles i and j. The MATLAB function '*mscohere*' was used to implement the above formula [53], employing Welch's overlapped averaged periodogram method with a Hanning window length of 2000 samples (corresponding to 1 s) and 50% overlap [54], [55]. The length of Welch's periodogram was set equal to 2048 samples to achieve a spectral resolution of approximately 1 Hz. The coherence function $C_{i,j}(f)$ ranges from 0 to 1, where 0 indicates no coherence and 1 indicates perfect coherence at frequency f. The coherence function was then smoothed by means of a moving average filter (centered sliding window of length $L_{mov} = 20$) for the following analyses. An example of an IMC matrix is shown in **Figure 2B**;

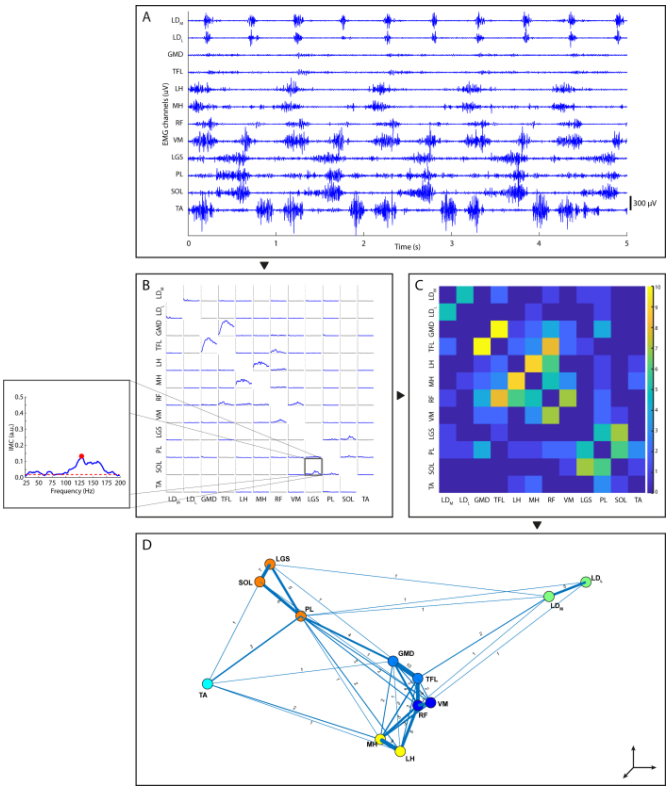

Fig. 2. Pipeline for muscle-network graph extraction. (A) Example of (pre-processed) EMG signals recorded, during a walking task, from 12 muscles of a representative subject. (B) InterMuscular Coherence (IMC) of each pair of muscles displayed in the range of frequencies: 25 Hz-200 Hz. The zoom on the subplot "LGS-SOL" of panel (B) shows the IMC peak detection (red dot) and the Confidence Limit (CL) of coherence (red dashed line). (C) Weighted intermuscular adjacency matrix of coherence: each element of the (symmetrical) matrix A represents a quantized value of the IMC peak (k = 10 quantization levels are present). (D) 3D graph representing the muscle network of the subject (see Supplementary Material for a 3D animation). The "nodes" of the graph are the muscles. The "edges" between nodes (connections or links between muscles) show heavier "weights" when higher coherence peaks between muscles is present (in the walking task of the subject). The muscles belonging to a cluster are represented with the same color (6 clusters can be recognized in this case). LD_M Longissimus Dorsii of the more affected side; LD_L Longissimus Dorsii of the less affected side; GMD gluteus medius; TFL tensor fasciae latae; LH lateral hamstring; MH medial hamstring; RF rectus femoris; VM vastus medialis; LGS lateral gastrocnemius; PL peroneus longus; SOL soleus; and TA tibialis anterior.

b) *Matrix of IMC peaks:* for each pair of muscles (i, j), the peak of coherence ($IMC_{PEAK_{i,j}}$) was estimated as the maximum value of the IMC function $C_{i,j}(f)$ [34], [55] considering the range of frequencies from 25 Hz to 200 Hz (which contains approximately 90% of the EMG signal power) [56]. Many studies, especially those estimating Cortico-Muscular Coherence (CMC), proposed to analyze the typical EEG frequency bands, such as β band (15 Hz - 30 Hz) and low γ band (30 Hz - 60 Hz) [57], [58], [59]. In this study, since we are considering EMG-EMG coherence, the frequency band of interest was extended to higher frequencies to analyze as much of the EMG spectrum as possible. The matrix of the peak values of coherence (IMC_{PEAK}) was obtained (size: 12×12, being N the number of muscles analyzed). The choice of IMC_{PEAK} parameter was derived from

extensive literature review and supported by methodological studies demonstrating its reliability and equivalence to spectrum-based alternatives [34], [52], [55], [60], [61], [62], [63]. Notice that this matrix is symmetrical. The values on the main diagonal were discarded: a coherence equal to 1 would be obtained from 2 identical EMG signals of the same muscle (when $i = j$), but the concept of IMC would lose its meaning;

c) *Weighted Intermuscular Adjacency Matrix of Coherence* (A)*:* first, IMC_{PEAK} values below the confidence limit were set to zero to remove low coherence values attributable to noise. The Confidence Limit (CL) for intermuscular coherence was identified with a significance level (α) set equal to 0.05 by using **Equation (2)**:

$$CL = 1-\alpha^{\frac{1}{L-1}}, where\ L = floor\left(\frac{total\ signal\ length}{WL}\right) \quad (2)$$

being L the number of disjoint segments used to calculate the coherence [64]. In our study, WL (i.e., window length) was set equal to 2000. Coherence values exceeding CL were considered significant connections between muscle nodes. Significant coherence peak values were then quantized using k-means clustering with $k = 10$ clusters. This number was selected empirically, considering that node degree in muscle networks is typically much smaller than N–1 ($N = 12$ muscles recorded) and validated considering a sensitivity analysis in which different values of k were tested. For each candidate k, we quantified the proportion of variance in the dicretized coherence signal explained relative to the continous coherence signal. The MATLAB function '*kmeans*' was used to implement k-means clustering, considering $n = 50$ replicates and squared Euclidean as distance metric. Clustering centroids were sorted in ascending order to define k discrete coherence intervals, with each centroid serving as the lower bound (i.e., quantization level) of its respective interval. Finally, each significant coherence value was assigned an integer weight $w \in 1, \ldots, k$ according to its cluster membership, yielding the weighted adjacency matrix A. This procedure produces a symmetric, weighted intermuscular adjacency matrix in which edge weights reflect the relative strength of statistically significant intermuscular coherence. An example of matrix A is shown in **Figure 2C**;

d) *Muscle network - graph drawing:* a muscle network is constructed by building the (undirected weighted) graph relative to the obtained matrix A through a force-based approach [65]. The attractive and repulsive forces defined, in force-based algorithms, position the nodes/muscles in the spatial configuration that brings them as close as possible when they are connected by an edge with high weight (i.e., high intermuscular coherence) and moves them farther apart when they are connected by an edge with low weight (i.e., low intermuscular coherence). Thus, the resulting network will consist of N nodes (N = number of muscles involved in the study), and a variable number of edges depending on the weights $A_{i,j}$. The '*graph*' function of MATLAB was used to draw 3D graphs. Since this is an iterative algorithm, the number of iterations (n_{iter}) was set to 1000, allowing for a good balance between a low "temperature" value reached (a metric that describes the freedom of the nodes to move in the graph) and a sufficiently low computational cost [66]. An example of a 3D (muscle network) graph is reported in **Figure 2D**;

e) *Muscle network - graph clustering:* to study how muscles collaborate during the walking task, it is useful to understand how the nodes position themselves in space and interpret the structure of the network by partitioning the set of analyzed muscles into clusters. Then, each cluster can be represented by a different color (as shown in **Figure 2D**). Since each connection has a weight proportional to the level of intermuscular coherence between the nodes/muscles involved, we expect that the most densely connected muscles will be grouped together in a single cluster (and well separated from the remaining clusters). Each cluster can be interpreted as a group of muscles that are coordinated in the movement (i.e., whose joint activation is related to the same motor function). To achieve this partitioning/clustering, we used the Louvain method [67] to separate the generated muscle-network graph into muscle clusters that reflect the different functional activities of the involved muscles. Let c_i be the cluster to which node i is assigned. The Louvain method is an iterative algorithm that maximizes a parameter called modularity (Q) [68], defined as in **Equation (3)**:

$$Q = \frac{1}{2m}\sum_{i,j}\left[A_{i,j} - \frac{k_i k_j}{2m}\right]\delta\left(c_i, c_j\right) \quad (3)$$

where $A_{i,j}$ is the adjacency matrix of the graph, k_i and k_j are the degrees of nodes i and j, m is the total number of edges in the graph, and $\delta\left(c_i, c_j\right)$ is the Kronecker delta, which is 1 if nodes i and j are in the same cluster of muscles and 0 otherwise. This metric allows us to quantify the strength of the proposed division into clusters and, in this work, it can be interpreted as a parameter that reflects the separability of muscle groups that activate synergistically. A limitation of the Louvain method is that it is based on a stochastic algorithm, and its results heavily depend on the number of iterations and on the value of a resolution parameter that regulates the size and number of the clusters in the network. When the resolution is high, smaller clusters are more likely to be formed. This resolution parameter is often chosen arbitrarily depending on the application for which the method is used. To overcome this problem, in accordance with the study by Hug et al. [69], we partitioned the network using a consensus clustering algorithm [70]. Consensus clustering provides a method that represents the consensus across multiple runs of a clustering algorithm to determine the number of clusters in the network and to assess the stability of the discovered clusters. The proposed consensus clustering framework is developed in multiple iterative steps:

i) Define a set of resolutions including all plausible values around 1.0 (i.e., from 0.5 to 1.5 with a step of 0.0001). In this way, we will have $n_{part} = 10000$ possible resolution values;

ii) Execute the Louvain method using the MATLAB implementation included in the GenLouvain algorithm (https://github.com/GenLouvain/GenLouvain) [71], for each possible resolution value, saving the set of partitions (n_{part}) and the associated modularity (Q) values;

iii) Create the agreement matrix D whose elements are the percentage of partitions in which the node i is clustered together with the node j (size: N×N; in this work: 12×12). Additionally, define a threshold τ that indicates the minimum percentage of partitions for which a pair of muscles can be considered stably connected as described by **Equation (5)**:

$$\tau = 0.8 * n_{part} \tag{4}$$

Considering the node i, this is aggregated into the same cluster of all the nodes j for which $D(i, j) > \tau$ (agreement obtained in more than 80% of the total partitions). If a node does not meet the imposed condition in any case, it is assigned to a solitary cluster. In other words, considering the node i, if $D(i, j) \leq \tau$ for every $j \neq i$, then i is assigned to a solitary cluster;

iv) The clusters generated by thresholding the matrix D provide a "consensus partition". Thus, this partition is independent from the choice of the resolution parameter.

3) **Graph metrics.** To obtain quantitative outcome measures and understand the information that the muscle-network graph can offer in the study of motor control during gait, we used the following four metrics: two global metrics (modularity and density) and two local metrics (node strength and local cluster coefficient).

a) *Modularity* (M)*:* modularity was already partially introduced in the previous section through **Equation (3)**, as the metric that needs to be maximized to obtain the node/muscle color-coding in the graph, for representing the different muscle clusters. As previously mentioned, modularity describes how easily a network can be divided into clusters. Indeed, high modularity reflects a high number of connections, with high weights, within clusters (pairs of muscles with high EMG-EMG coherence and IMC peak values), accompanied by a low number of connections, with low weights, between clusters (pairs of muscles with low IMC peak values). Modularity can assume values between 0 and 1, with a modularity of 0 indicating a random clustering of the graph [68];

$$D = \frac{2E}{N(N-1)} \tag{5}$$

b) *Density* (D)*:* density is defined as the ratio between the number of actual edges in the network and the maximum theoretical number of edges that a graph with N nodes can have [69]. In the case of undirected graphs, density is defined as in **Equation (5)**: where E is the number of edges in the graph and N is the number of nodes/muscles. Density can assume values between 0 and 1. A small graph density reflects a small number of muscle pairs characterized by a significant IMC value.

c) *Node strength* (s)*:* it quantifies the total strength of functional coupling for each muscle and it is computed as the sum of edge weights (w) connected to the i-th node i [28], [72].

d) *Local clustering coefficien* (c)*:* it is calculated as the ratio of existing edges between the i-th node's neighbors to the maximum possible connections between them [73]. In the case of weighted undirected graphs, c is defined as in **Equation (6)**:

$$c_i = \frac{1}{deg(i)(\deg(i)-1)} \sum_{j,k} (w'_{ij} w'_{jk} w'_{ki})^{1/3} \tag{6}$$

where the indices j and k denote two neighbors of the i-th node such that the triplet (i, j, and k), while w'_{ij}, w'_{jk}, and w'_{ki} represent the weights of the edges connecting each pair of nodes within this triad. These weights are normalized by the maximum edge weight in the network [73]. Local clustering coefficient characterizes the tendency of a muscle's neighboring nodes to be mutually interconnected, reflecting localized coordination patterns. These metrics allow us to examine how individual muscles contribute to the overall network organization.

Finally, to evaluate the clinical validity of the muscle-network global metrics (i.e., modularity and density), their agreement with the clinical score (UPDRS-III) assigned to each PD patient was analyzed. Agreement was quantified as Percent Agreement (PA), defined as the number of agreements divided by the total number of PD patients.

D. Statistical Analysis

A 2-sample Student's t-test (2 tails) was used to compare the anthropometric characteristics of PD patients and controls. A paired Student's t-test (2 tails) was used to compare the UPDRS-III scores of PD patients at T_0 and T_2.

The homogeneity of variances among groups was verified, for all the analyzed parameters, using Levene's F test. Subsequently, the differences among groups (PD patients, at the 3 time points, and controls) were analyzed using a Mixed Model based on Repeated Measure One-way Analysis of Variance (*rm-1-way* ANOVA), with timepoints (PD at T_0, T_1, and T_2) as within-subjects factor and group (PDs and Controls) as between-subjects factor. The analysis was repeated for each global and local graph metric, separately. Therefore, "*Group*" was the independent variable, and the graph metric (i.e., modularity, density, node strength, and local clustering coefficient) was the dependent variable. *Post-hoc* analyses and multiple comparisons among patients before surgery (PD at T_0), 3 months after surgery (PD at T_1), 12 months after surgery (PD at T_2), and controls were performed using Bonferroni adjustments. The effect size of statistically significant differences was computed by means of the Hedges' g statistic [74]. The significance level α was set at 0.05 for all analyses, and all variables were expressed as mean ± standard deviation across the population. All statistical analyses were performed using a standard software package (SPSS Statistical Software, version 28.0, SPSS Inc., Chicago, IL).

TABLE I
ANTHROPOMETRIC (AND CLINICAL) CHARACTERISTICS OF PARKINSON'S DISEASE (PD) PATIENTS AND CONTROLS

	GENDER	AGE (*years*)	HEIGHT (*cm*)	MASS (*kg*)	CLINICAL ASSESSMENT TIME	YEARS AFTER PD DIAGNOSIS	HOEHN & YAHR SCALE[2]	UPDRS-III[2]
PD patients[1] (*n*=27)	19 M, 8 F	57.4±8.0	171.9±11.0	74.4±2.7	Baseline before DBS (T_0)	11.19±0.63	Stage I: 4 (15%) Stage II: 22 (81%) Stage III: 1 (4%)	**19.4 ± 1.8*****
					12 months after DBS (T_2)	12.32±0.64	Stage I: 19 (70%) Stage II: 7 (26%) Stage III: 1 (4%)	**10.2 ± 1.0*****
Controls (*n*=30)	12 M, 18 F	55.0±8.5	167.9±8.1	74.1±3.4	N/A	N/A	N/A	N/A

[1]*The PD anthropometric characteristics reported were assessed at baseline.* [2]*The PD clinical scores reported (Hoehn & Yahr scale and UPDRS-III) were assessed in "best-ON" conditions. PD: Parkinson's Disease, M: Males, F: Females, UPDRS-III: Unified Parkinson's Disease Rating Motor Subscale, N/A: Not Applicable. Continuous variables are reported as mean ± standard deviation of the population. Statistically significant differences are represented through asterisks (*** p <0.001) and highlighted in bold. Group comparisons were tested using 2-samples Student's t-test, while within-PD UPDRS-III changes were tested using paired Student's t-test.*

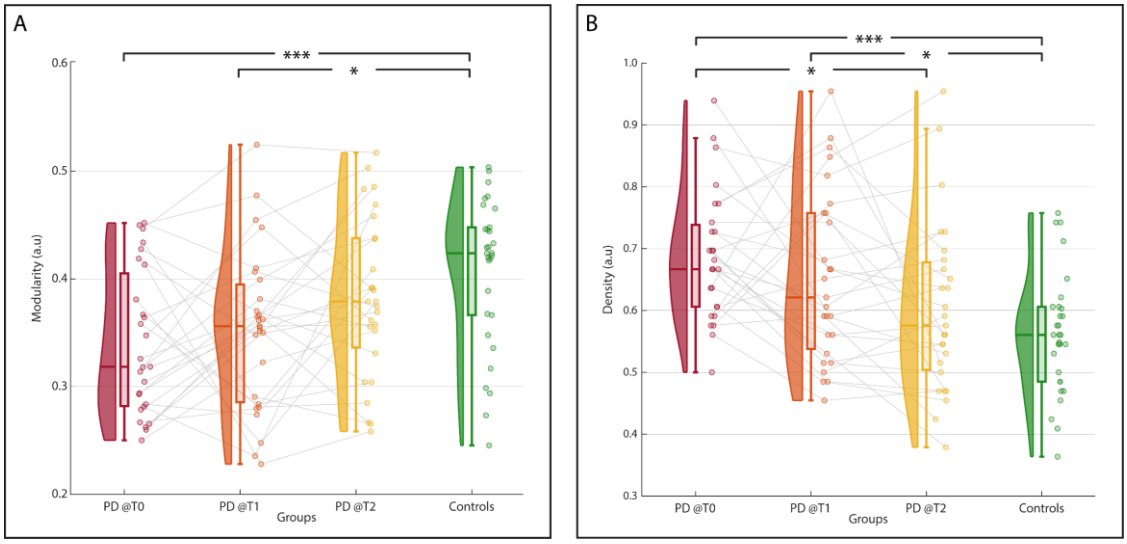

Fig. 3. Comparison of muscle-network metrics among groups. Raincloud plots of the graph metrics: Modularity (panel A) and Density (panel B). In each panel the metric is compared among PD patients at baseline (T_0, in red), at 3 months after DBS (T_1, in orange), at 12 months after DBS (T_2, in yellow), and controls (in green). For each group, the raincloud plot shows, sequentially, the data distribution (split-half violin plot), a standard visualization of central tendency with a boxplot (representing minimum, 25th percentile, median, 75th percentile, and maximum), and raw jittered data points of each specific individual (scatter plot). Group differences were analyzed using a mixed-model repeated-measure one-way ANOVA with timepoints (T_0, T_1, T_2) as within-subjects factor and group (PD and Controls) as between-subjects factor, followed by Bonferroni-corrected post-hoc comparisons. Asterisks represent statistically significant differences between groups, with $p < 0.05$ ($*$) or $p < 0.001$ ($***$).

III. RESULTS

Three out of thirty PD patients who underwent the gait examinations were excluded from the final data analysis since they had orthopedic surgery during the follow-up (between T_1 and T_2). This was chosen, as declared in our protocol, to avoid comorbidities that could potentially alter gait patterns. Therefore, 27 PD patients (at 3 time points) and 30 controls were further analyzed. Anthropometric characteristics of PD patients and controls are reported in **Table I**, as well as PD clinical data before DBS surgery (baseline T_0) and at 1 year after DBS surgery (T_2).

Two-samples Student's *t*-test revealed no statistically significant differences between PD patients and healthy controls for age, height, and weight. A significant reduction in the UPDRS-III motor scale was observed, from an average value of 19.4 points (at T_0 during best pharmacological time window) to 10.2 points (at T_2 during best pharmacological time window and optimal DBS programming settings), revealing that PD patients clinically improved their motor performance 1 year after DBS neurosurgery (paired Student's *t*-test, $p < 0.0001$, $g = 1.19$). This clinical improvement can also be appreciated considering the Hoehn and Yahr (H&Y) scale [45]. Indeed, before DBS, a large majority of patients (81%) belonged to Stage II, while one year after DBS, a large number of patients (70%) belonged to Stage I.

After the construction of the muscle-network graph of each subject (as described in the Methods section), four metrics were calculated: modularity, density, node strength, and local clustering coefficient. The average values of these metrics are compared among the PD group (at the three time points T_0,

TABLE II
COMPARISON OF MUSCLE-NETWORK GLOBAL METRICS AMONG PARKINSON'S DISEASE PATIENTS AT THE THREE DIFFERENT TIME POINTS (T_0, T_1, AND T_2) AND CONTROLS

Global graph metrics		Parkinson's Disease patients			Controls	*1-way* ANOVA Group (*p*-value)
		T_0	T_1	T_2		
MODULARITY		$0.34 \pm 0.07^{*}$	$0.35 \pm 0.07^{\dagger}$	0.38 ± 0.07	$0.41 \pm 0.07^{*,\dagger}$	**0.002**
Post-hoc *p*-values[1]	T_0 vs. Controls	**0.003**			**0.003**	
	T_1 vs. Controls		**0.037**		**0.037**	
	T_2 vs. Controls			1.0	1.0	
	T_0 vs. T_1	1.0	1.0			
	T_0 vs. T_2	0.27		0.27		
	T_1 vs. T_2		0.37	0.37		
DENSITY		$0.69 \pm 0.10^{*,\ddagger}$	$0.65 \pm 0.14^{\dagger}$	$0.60 \pm 0.14^{\ddagger}$	$0.56 \pm 0.10^{*,\dagger}$	**< 0.0009**
Post-hoc *p*-values[1]	T_0 vs. Controls	**0.0009**			**0.0009**	
	T_1 vs. Controls		**0.034**		**0.034**	
	T_2 vs. Controls			1.0	0.99	
	T_0 vs. T_1	1.0	1.0			
	T_0 vs. T_2	**0.049**		**0.049**		
	T_1 vs. T_2		0.36	0.36		

[1]*Post-hoc comparisons with Bonferroni adjustments. T_0: PD patients in baseline conditions (before DBS); T_1: PD patients, 3 months after DBS; T_2: PD patients, 12 months after DBS. Metrics' values are reported as mean ± standard deviation of the population. Group differences were analyzed using a mixed-model repeated-measure one-way ANOVA with timepoints (T_0, T_1, T_2) as within-subjects factor and group (PD and Controls) as between-subjects factor. Asterisks (*), daggers (†) and double daggers (‡) represent statistically significant differences in the T_0 vs. Controls, T_1 vs. Controls, and T_0 vs. T_2 comparisons, respectively. P-values are highlighted in bold if p<0.05.*

T_1, and T_2) and the reference population of healthy subjects. More specifically, **Table II** details the improvements in the density and modularity metrics from the pre-surgery condition (T_0) up to 12 months post-surgery (T_2). Indeed, a clear trend of the PD patients values toward the reference values of the Control group can be noted. Mixed-model repeated-measure one-way ANOVA revealed significant differences between T_0 and Controls (Modularity: $p = 0.003$, $g = 0.97$; Density: $p = 0.0009$, $g = 1.24$) and between T_1 and. Controls (Modularity: $p = 0.037$, $g = 0.75$; Density: $p = 0.034$, $g = 0.77$). Furthermore, confirming the improvement of the metrics, there is a borderline difference between T_0 and T_2 ($p = 0.049$, $g = 0.68$) in the density of the graphs. No significant differences emerged at T_2 vs. Controls ($p = 1.00$), indicating that PD patients' muscle network characteristics normalized to those of healthy controls at 12 months after DBS surgery. In general, decreased network density, coupled with increased modularity, reflects a more refined and specialized motor control strategy, characterized by selective muscle activation patterns. The distributions of the metrics and their changes during the DBS follow-up are shown in **Figure 3**. In addition to the improving trend across the whole PD population, this figure also shows the longitudinal assessment of each PD patient (through grey trend lines connecting the colored circular dots, where each dot represents a single patient at a specific time point).

Table III details the average node strength and local clustering coefficient metrics from the pre-surgery condition (T_0) up to 12 months post-surgery (T_2) with the indication of the statistically significant differences. Node-level analyses revealed a clear trend: PD patient values shifted toward Control group reference values after DBS surgery, indicating reduced individual muscle connectivity and more structured muscle coordination. Mixed-model repeated-measures one-way ANOVA on node strength showed significant differences between PD patients and controls for all muscles ($p < 0.005$). Local clustering coefficient analyses detected statistically significant differences ($p < 0.021$) for all muscles except distal muscles (PL, SOL, and TA) and TFL. Node-level metrics during DBS follow-up are presented in **Supplementary Figures 1** (node strength) and **Supplementary Figure 2** (local clustering coefficient).

A general overview of the graphs obtained for PD patients at the three time points and for healthy subjects is shown in **Figure 4**. These networks were generated by calculating the average adjacency matrices among the populations and extracting the corresponding graphs. It can be noted that, even in the case of the average graphs, the extracted global parameters (modularity and density) follow the trend described in **Figure 3** and **Table II** (Modularity: $T_0 = 0.37$, $T_1 = 0.40$, $T_2 = 0.42$, Controls= 0.45; Density: $T_0 = 0.71$, $T_1 = 0.68$, $T_2 = 0.65$, Controls= 0.59). We observe that the pattern of clusters found consistently presents six muscle groups, remaining unchanged across the four networks. This confirms that the roles of the muscle groups (associated with the clusters) and the muscle activation strategies are not substantially modified in PD patients. However, in Panel A of **Figure 4** (representing T_0), a high number of edges (high density) connect distinct clusters and the clusters tend to be closer to each other (low modularity). The number of edges decreases, and the clusters progressively distance themselves when moving from Panels B

TABLE III
COMPARISON OF MUSCLE-NETWORK LOCAL METRICS AMONG PARKINSON'S DISEASE PATIENTS AT THE THREE DIFFERENT TIME POINTS (T_0, T_1, AND T_2) AND CONTROLS

Local graph metrics		Parkinson's Disease patients			Controls	*1-way* ANOVA Group (*p*-value)
		T_0	T_1	T_2		
NODE STRENGTH						
Muscles	LD_M	$26.7 \pm 7.0^{*,**,\dagger}$	$21.4 \pm 10.9^{*}$	$20.6 \pm 7.6^{**,\dagger\dagger}$	$14.7 \pm 6.9^{\dagger,\dagger\dagger}$	**<0.0001**
	LD_L	$25.7 \pm 9.3^{\dagger}$	$23.2 \pm 9.9^{\dagger\dagger}$	$23.1 \pm 9.4^{\dagger\dagger\dagger}$	$16.2 \pm 7.1^{\dagger,\dagger\dagger,\dagger\dagger\dagger}$	**0.001**
	GMD	$41.9 \pm 8.0^{*,\dagger}$	36.4 ± 10.3	$32.8 \pm 10.2^{*}$	$30.5 \pm 8.9^{\dagger}$	**<0.0001**
	TFL	$42.4 \pm 8.6^{*,**,\dagger}$	$36.6 \pm 9.2^{*,\dagger\dagger}$	$34.1 \pm 10.7^{**,\dagger\dagger}$	$27.5 \pm 8.6^{\dagger,\dagger\dagger,\dagger\dagger\dagger}$	**<0.0001**
	LH	$31.2 \pm 8.8^{\dagger}$	26.4 ± 7.5	25.5 ± 8.1	$23.3 \pm 5.8^{\dagger}$	**0.005**
	MH	$32.5 \pm 10.2^{*,\dagger}$	$27.3 \pm 8.1^{\dagger\dagger}$	$25.0 \pm 7.5^{*}$	$20.8 \pm 7.2^{\dagger,\dagger\dagger}$	**<0.0001**
	RF	$39.3 \pm 7.8^{\dagger}$	$36.5 \pm 9.4^{\dagger\dagger}$	34.7 ± 11.1	$29.9 \pm 6.1^{\dagger,\dagger\dagger}$	**<0.0001**
	VM	$39.2 \pm 8.3^{*,**,\dagger}$	$28.5 \pm 8.1^{*}$	$26.6 \pm 9.6^{**}$	$23.9 \pm 7.6^{\dagger}$	**<0.0001**
	LGS	$27.1 \pm 9.7^{*,\dagger}$	18.7 ± 7.8	$22.8 \pm 10.9^{*,\dagger\dagger}$	$14.8 \pm 7.4^{\dagger,\dagger\dagger}$	**<0.0001**
	PL	$30.2 \pm 9.2^{*,**,\dagger}$	$22.3 \pm 8.3^{*}$	$21.4 \pm 9.3^{**}$	$21.1 \pm 10.6^{\dagger}$	**0.002**
	SOL	$27.3 \pm 9.6^{\dagger}$	$25.7 \pm 10.4^{\dagger\dagger}$	20.7 ± 9.4	$18.7 \pm 7.7^{\dagger,\dagger\dagger}$	**0.004**
	TA	$24.0 \pm 10.7^{*,**,\dagger}$	$15.7 \pm 9.1^{*}$	$13.8 \pm 9.9^{**}$	$12.6 \pm 8.7^{\dagger}$	**0.001**
LOCAL CLUSTERING COEFFICIENT						
Muscles	LD_M	$0.17 \pm 0.05^{*,\dagger}$	0.19 ± 0.07	$0.21 \pm 0.04^{*}$	$0.24 \pm 0.07^{\dagger}$	**0.001**
	LD_L	$0.16 \pm 0.07^{*,**,\dagger}$	$0.20 \pm 0.07^{*}$	$0.23 \pm 0.06^{**}$	$0.22 \pm 0.07^{\dagger}$	**0.002**
	GMD	$0.24 \pm 0.07^{\dagger}$	0.24 ± 0.06	0.25 ± 0.06	$0.29 \pm 0.07^{\dagger}$	**0.027**
	TFL	0.24 ± 0.07	0.24 ± 0.05	0.25 ± 0.07	0.26 ± 0.05	0.57
	LH	$0.24 \pm 0.07^{\dagger}$	$0.25 \pm 0.05^{\dagger\dagger}$	$0.24 \pm 0.6^{\dagger\dagger\dagger}$	$0.30 \pm 0.06^{\dagger,\dagger\dagger,\dagger\dagger\dagger}$	**0.004**
	MH	$0.22 \pm 0.07^{\dagger}$	0.25 ± 0.06	$0.24 \pm 0.06^{\dagger\dagger}$	$0.29 \pm 0.05^{\dagger,\dagger\dagger}$	**0.003**
	RF	$0.24 \pm 0.06^{\dagger}$	0.26 ± 0.07	0.27 ± 0.08	$0.30 \pm 0.06^{\dagger}$	**0.018**
	VM	$0.25 \pm 0.06^{\dagger}$	0.26 ± 0.06	0.25 ± 0.07	$0.30 \pm 0.06^{\dagger}$	**0.021**
	LGS	$0.22 \pm 0.07^{\dagger}$	$0.21 \pm 0.06^{\dagger\dagger}$	$0.22 \pm 0.07^{\dagger\dagger\dagger}$	$0.28 \pm 0.07^{\dagger,\dagger\dagger,\dagger\dagger\dagger}$	**0.002**
	PL	0.21 ± 0.10	0.22 ± 0.08	0.21 ± 0.07	0.23 ± 0.07	0.81
	SOL	0.22 ± 0.06	0.22 ± 0.08	0.23 ± 0.07	0.25 ± 0.06	0.24
	TA	0.17 ± 0.06	0.19 ± 0.06	0.19 ± 0.07	0.22 ± 0.06	0.081

Values are reported as mean ± standard deviation. Group differences were analyzed using a mixed-model repeated-measure one-way ANOVA with timepoints (T_0, T_1, T_2) as within-subjects factor and group (PD, Controls) as between-subjects factor, followed by Bonferroni-corrected post-hoc comparisons. Asterisks (*, **, ***) denote statistically significant differences in T_0 vs. T_1, T_0 vs. T_2, and T_1 vs. T_2 comparisons; daggers (†, ††, †††) denote differences between PD patients at T_0, T_1, and T_2 vs. Controls. Abbreviations: LD_M Longissimus Dorsii of the more affected side; LD_L Longissimus Dorsii of the less affected side; GMD gluteus medius; TFL tensor fasciae latae; LH lateral hamstring; MH medial hamstring; RF rectus femoris; VM vastus medialis; LGS lateral gastrocnemius; PL peroneus longus; SOL soleus; and TA tibialis anterior.

(T_1) and C (T_2) until reaching the condition of the Controls in Panel D. This evolution is particularly evident for distal muscle clusters (TA, PL, SOL, and LGS), which progressively segregate from proximal muscles, reflecting increasing functional specialization.

Until now, we have mainly focused on the longitudinal changes of the whole experimental PD population (compared to the control group). However, we have also analyzed if each specific PD patient improved, based on the numerical values provided by the muscle-network graph metrics, as well as the level of agreement of these metrics with the clinical score assigned.

Therefore, **Figure 5** shows the behavior of each PD patient (i.e., their motor changes during the follow-up after DBS). The right panels of **Figure 5** represent the changes in modularity (**Figure 5A**) and density (**Figure 5C**) of the graph at 3 months after DBS compared to baseline (T_1–T_0), and at 12 months after DBS compared to baseline (T_2–T_0). Positive values of modularity changes (T_1–$T_0 > 0$ or T_2–$T_0 > 0$) indicate an improvement after DBS neurosurgery, reflecting increased functional specialization and selective activation patterns. Conversely, negative values indicate worsening motor control, characterized by simplified control strategies with reduced modularity and increased muscle co-contractions. The opposite applies to changes in density.

In particular, three groups of PD patients can be distinguished:

1. "Improved" group: patients who overall revealed modularity/density changes, after DBS stimulation, toward the reference values of the control group;
2. "Stable" Group: Patients Who Overall Revealed No Modularity/Density Changes After DBS Stimulation
3. "Not Improved" group: patients who overall revealed modularity/density changes, after DBS stimulation, away from the reference values of the control group.

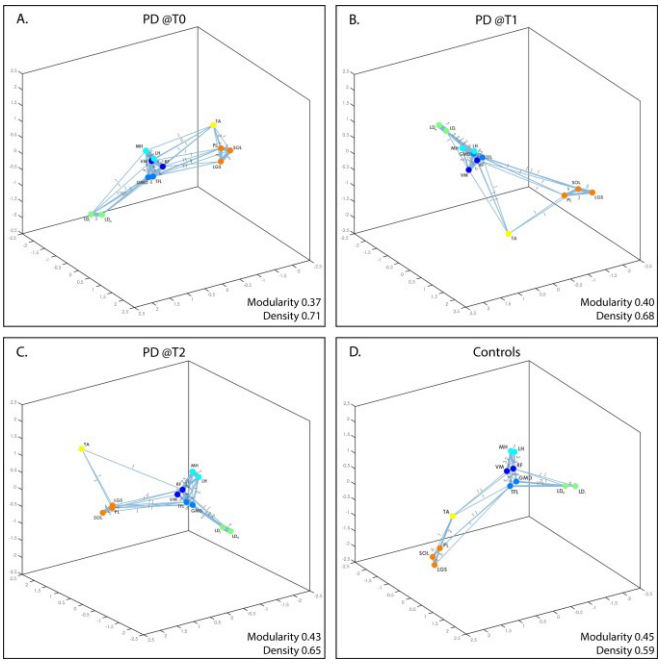

Fig. 4. Comparison of average muscle-network graphs among groups. PD at T_0, T_1, T_2, and controls are displayed in panel A, B, C and D, respectively. Abbreviations: LD_M Longissimus Dorsii of the more affected side; LD_L Longissimus Dorsii of the less affected side; GMD gluteus medius; TFL tensor fasciae latae; LH lateral hamstring; MH medial hamstring; RF rectus femoris; VM vastus medialis; LGS lateral gastrocnemius; PL peroneus longus; SOL soleus; and TA tibialis anterior.

Considering modularity (**Figure 5A**), 17 out of 27 patients improved, 9 did not improve, and 1 remained stable. Considering density (**Figure 5C**), 18 out of 27 patients improved, 6 did not improve, and 3 were stable. The right panels of **Figure 5** display the agreement between the modularity and UPDRS-III changes (**Figure 5B**) and between the density and UPDRS-III changes (**Figure 5D**). For both graph metrics, as well as for UPDRS-III, the relative change (T_2–T_0) between the 12-month assessment after DBS and baseline was considered. Overall, the proposed quantitative graph-derived metrics demonstrated good alignment with clinical assessment scales. Graph metrics changes tracked clinical improvement as measured by UPDRS-III, with percent agreements of 74.1% for modularity and 81.5% for density, suggesting that network-based parameters effectively capture motor function changes reflected in clinical assessment.

IV. Discussion

Numerous studies have contributed to the development of EMG signal analysis techniques aimed at assessing motor control strategies in both healthy individuals and pathological populations, such as post-stroke patients or individuals with Parkinson's Disease (PD) [75]. However, to the best of the authors' knowledge, this work is the first to integrate the concepts of muscle networks [76], intermuscular coherence [77], [78], [79], and graphs generated using a force-based approach [69] offering a new perspective on the theme. The goal of this study was to explore the potential of graph theory for evaluating gait coordination in PD patients following subthalamic nucleus Deep Brain Stimulation (DBS), by constructing a weighted network of the muscles primarily involved in locomotion.

An experimental population of 27 PD patients was evaluated at three separate time points (T_0 (ON medication), T_1 (ON medication with DBS activated), and T_2 (ON medication with DBS activated)) and compared to a control population of 30 healthy volunteers. This approach was employed to compare the patients' best-ON condition across the three time points. The selection of this approach was further justified by the consideration that many patients would have found it extremely difficult or even impossible to autonomously complete a 5-minute walking task while being OFF medication. To accurately identify a homogenous cohort, PD patients were enrolled in the study under strict inclusion criteria based on established clinical scales (i.e., the MMSE and FAB for the neuropsychological and behavioral evaluation, and the UPDRS-III and H&R scale for the clinical assessment).

Designed as a longitudinal study, the proposed analyses provide a comprehensive overview of the subjects' motor functional profile in the 12 months following the DBS implant. This approach can be crucial both for the global characterization of a study group and for tracking the progression of the disease in individual patients with objectivity, offering new interpretative tools to clinicians.

The innovation introduced by this study resides in the evaluation of the clinical validity of both the method and the parameters extracted. Specifically, both the global and the local parameters of the muscle-network graphs follow a unique trend: PD patients differ significantly from healthy controls at the initial time point (T_0), but demonstrate a gradual convergence towards the control group at 3 months (T_1) and then at 12 months (T_2) after the start of the electroceutical therapy, suggesting the effectiveness of DBS in improving PD motor symptoms. Direct comparison of the obtained results with existing literature is not easy, as previous studies have employed different methodologies [25], [58], [80], examined different tasks [53], [55], [57], or involved different populations. The trends observed in the proposed global metrics (i.e., modularity and density) align with the clinical evaluations provided by the UPDRS-III score for the majority of subjects (percent of agreement of 74.1% for modularity and 81.5% for density). This suggests that the information derived from the graphs could play a potentially significant role in supporting the clinical management of patients.

Traditional PD assessment using subjective scales like UPDRS-III suffers from rater variability, discrete scoring, and limited sensitivity. Network-based muscle coordination analysis provides a quantitative, neurophysiologically interpretable alternative. Network density and node strength quantify coordination efficiency by measuring connections among muscle pairs, revealing whether coordination is distributed or selective. Reduced density after DBS reflects fewer simultaneous co-activations, indicating a shift toward selective recruitment patterns. Modularity and local clustering coefficient assess muscle segregation into functional communities, providing insight into motor flexibility. Higher modularity indicates clear separation between synergistic groups, suggesting well-organized motor programs. Increased modularity post-DBS suggests restored functional specialization: distinct muscle synergies operate independently rather than merging into

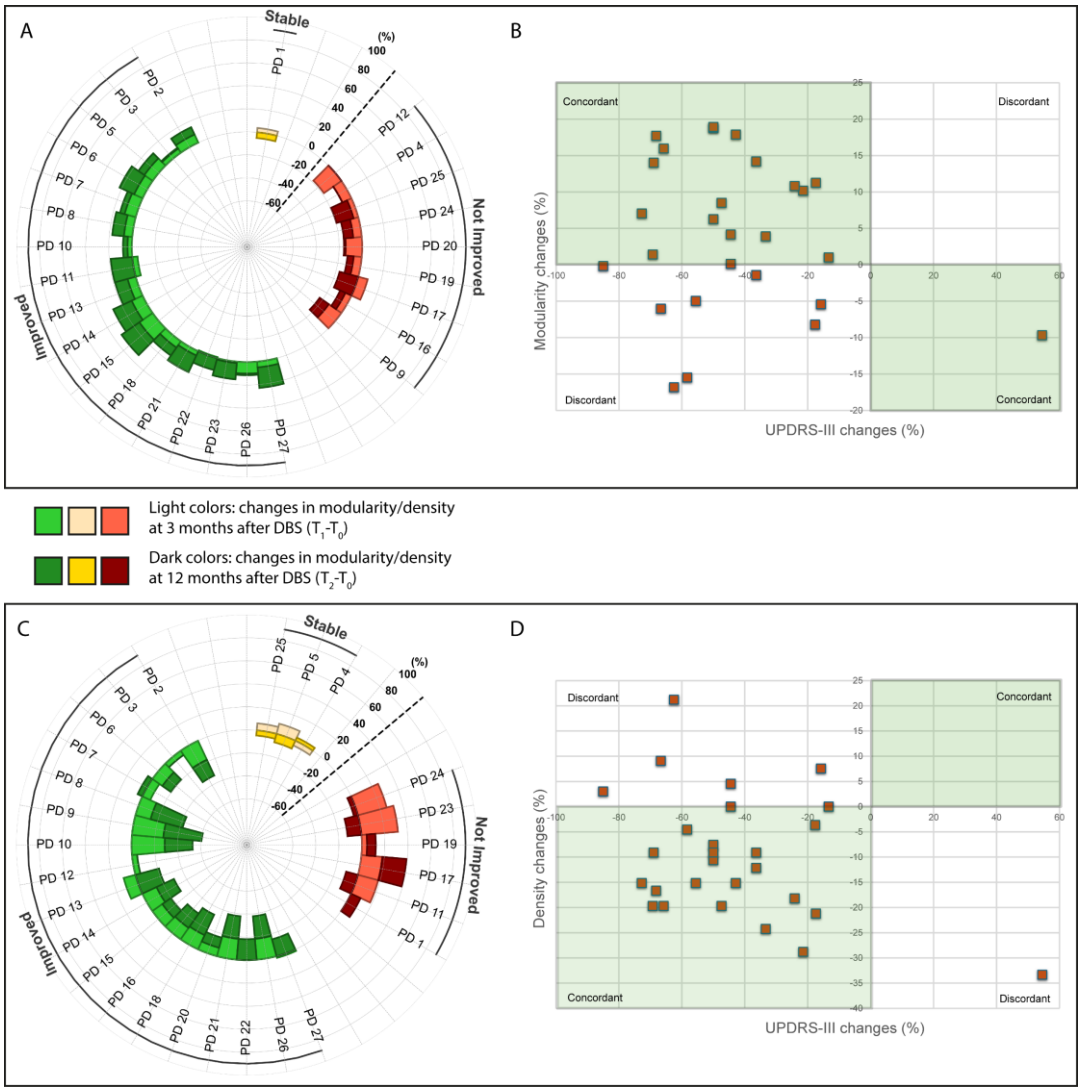

Fig. 5. Effects of DBS revealed by the muscle-network metrics (modularity and density) and agreement with the clinical score UPDRS-III. For each single PD patient, the circular bar diagram represents the relative changes in modularity (panel A) and density (panel C) of the muscle-network graph at 3 months after DBS with respect to baseline (T_1–T_0), and at 12 months after DBS with respect to baseline (T_2–T_0). A different color code is assigned to PD patients that improved (green), did not change (yellow), or worsened (red) after DBS. The concordance analysis between the muscle-network metrics and the clinical score UPDRS-III is shown in panel B for modularity and in panel D for density, respectively. In particular, the UPDRS-III relative changes T_2–T_0 are displayed on the x-axis, while the correspondent changes in modularity/density of the graph are represented on the y-axis (each square represents a PD patient). The quadrants showing an agreement between the modularity/density metrics and the UPDRS-III clinical score are highlighted through a light-green transparent rectangle.

global co-contraction. These network metrics enable objective treatment monitoring, patient stratification, and early detection of motor decline. Compared to UPDRS-III, they offer continuous, objective measurement sensitive to subclinical changes without rater bias.

Focusing on the assessment of muscle coordination during gait, one of the state-of-the-art methodologies is the use of muscle synergies. Despite its extensive use [81], [82], [83], this approach presents several challenges, including the difficulty of determining the number of synergies unambiguously and the numerous methodological choices required, which reduce the comparability of results across different studies. Our method offers a potential alternative to muscle synergies, emphasizing the simplicity of the extracted metrics and the visual and graphical impact, which may be more immediately interpretable by clinicians. In this regard, a potential future development of this work could involve a direct comparison between the two methods on the same population.

As shown in **Figure 4**, the clustering pattern obtained from the muscle networks largely aligns with the results found using muscle synergies [84], [85]. Specifically, the six identified clusters include muscles that are consistently grouped with respect to the anatomical segments of the trunk and lower limbs recruited in the locomotion task. In other words, there is a clear correspondence between each identified cluster and a specific gait biomechanical function. In particular:

- Cluster 1 (LD_M/LD_L) controls the trunk position in the frontal plane at heel strike;
- Cluster 2 (TFL/GMD) controls the hip joint stabilization during the heel strike and load acceptance phase;
- Cluster 3 (VM/RF) controls the knee joint stabilization during stance;

- Cluster 4 (MH/LH) controls the leg deceleration at the end of the swing phase;
- Cluster 5 (TA) controls the forefoot clearance during the swing phase and foot regulation during the first rocker;
- Cluster 6 (LGS/PL/SOL) controls the propulsion at mid and terminal stance.

The muscle network method provides additional insights by visualizing the interactions among the identified functional groups. Specifically, certain clusters (e.g., Cluster 2 and Cluster 3) are in closer proximity compared to others that are far away (e.g., Cluster 1 or Cluster 5), suggesting a tighter collaboration during specific phases of the gait cycle. Additionally, a greater number of connections and a more compact graph structure are noted in PD patients. This observation can be interpreted as a more widespread muscle co-activation in individuals affected by a neuropathological condition, accompanied by a higher average intermuscular coherence, as previously reported in the literatures [53] and [57]. These observations are substantiated by the obtained results: PD patients prior to the DBS intervention (time-point T_0) exhibit significantly higher density and lower modularity compared to healthy subjects. The density decreases—and the modularity increases—at the two subsequent time points (3 months post-intervention, T_1; and 12 months post-intervention, T_2), progressively approaching the reference parameters derived from healthy individuals. Considering the results obtained, we can hypothesize that the proposed metrics may hold significant clinical validity. Specifically, an increased network density, coupled with reduced modularity, reflects a less refined and simplified motor control strategy, characterized by widespread and pronounced muscle co-contractions.

A limitation in the use of surface electromyography can be the presence of crosstalk [86]. Compared to tasks involving the upper limb, where motor control is actuated by numerous small muscles, the impact of this issue is expected to be mitigated during gait, which is mainly actuated by recruiting the (larger) muscles of the lower limbs [87] and trunk. However, due to the anatomical positioning and structure of certain muscles involved (e.g., the TFL/GMD pair), intermuscular coherence values for certain subjects and muscle pairs may have been slightly influenced by crosstalk. An additional limitation of this study concerns the signal acquisition system. To obtain a comprehensive evaluation of motor control of the trunk and lower limb, we decided to prioritize the acquisition of a complete unilateral muscle set over a potential bilateral acquisition. However, in the study of pathologies that can be purely unilateral - such as Parkinson's disease at the early stages [88] - it could be highly informative to analyze the differences in control strategies between the two limbs. Future research could deeper investigate this aspect. Moreover, the adjacency matrix was computed using maximum IMC peaks per muscle pair [52], [55], [60], [61], [62], [63]. Although this approach has demonstrated reliability comparable to spectrum-based measures [34] it inherently discards spectral structure information. Alternative network construction methods using band-limited mean coherence or full-spectrum measures could provide complementary insights into the frequency-specific organization of motor control and represent an important direction for future methodological refinement. Then, this study employed fixed $k = 10$ quantization of muscle coherence, a choice that could potentially influence edge-weight distributions and derived network metrics. Future studies should examine continuous weighting approaches or conduct sensitivity analyses across different k values to establish methodological robustness.

Finally, an intriguing extension of this method could be the dynamic generation of muscle networks, with the objective of analyzing muscle interactions in each sub-phase of the gait cycle and providing a more detailed description of the biomechanical functions of the sampled muscle groups.

V. Conclusion

This study revealed that graph theory applied to EMG may be a sensitive framework for characterizing gait coordination in PD patients undergoing STN-DBS. Results suggest that graph-based EMG metrics may serve as quantitative markers of motor control. In particular, increased network density combined with reduced modularity appears to reflect a less refined, more stereotyped control strategy with widespread muscle co-contractions.

References

[1] S. A. Schneider and R. N. Alcalay, "Neuropathology of genetic synucleinopathies with Parkinsonism: Review of the literature," *Movement Disorders*, vol. 32, no. 11, pp. 1504–1523, Nov. 2017, doi: 10.1002/mds.27193.

[2] P. Mazzoni, B. Shabbott, and J. C. Cortes, "Motor control abnormalities in Parkinson's disease," *Cold Spring Harbor Perspect. Med.*, vol. 2, no. 6, Jun. 2012, Art. no. a009282, doi: 10.1101/cshperspect.a009282.

[3] N. Giladi, F. B. Horak, and J. M. Hausdorff, "Classification of gait disturbances: Distinguishing between continuous and episodic changes," *Movement Disorders*, vol. 28, no. 11, pp. 1469–1473, Sep. 2013, doi: 10.1002/mds.25672.

[4] J. Nonnekes, A. H. Snijders, J. G. Nutt, G. Deuschl, N. Giladi, and B. R. Bloem, "Freezing of gait: A practical approach to management," *Lancet Neurol.*, vol. 14, no. 7, pp. 768–778, Jul. 2015, doi: 10.1016/s1474-4422(15)00041-1.

[5] M. J. Armstrong and M. S. Okun, "Diagnosis and treatment of Parkinson disease: A review," *JAMA*, vol. 323, no. 6, p. 548, Feb. 2020, doi: 10.1001/jama.2019.22360.

[6] A. Suppa, M. Bologna, A. Conte, A. Berardelli, and G. Fabbrini, "The effect of L-dopa in Parkinson's disease as revealed by neurophysiological studies of motor and sensory functions," *Expert Rev. Neurotherapeutics*, vol. 17, no. 2, pp. 181–192, Feb. 2017, doi: 10.1080/14737175.2016.1219251.

[7] G. Deuschl et al., "European academy of neurology/movement disorder society–European section guideline on the treatment of Parkinson's disease: I. invasive therapies," *Eur. J. Neurol.*, vol. 29, no. 9, pp. 2580–2595, Sep. 2022, doi: 10.1111/ene.15386.

[8] G. Deuschl et al., "Deep brain stimulation of the subthalamic nucleus for the treatment of Parkinson's disease," *Lancet Neurol.*, vol. 8, no. 1, pp. 67–81, Jan. 2009, doi: 10.1016/S1474-4422(08)70291-6.

[9] D. Tan, M. Danoudis, J. McGinley, and M. E. Morris, "Relationships between motor aspects of gait impairments and activity limitations in people with Parkinson's disease: A systematic review," *Parkinsonism Rel. Disorders*, vol. 18, no. 2, pp. 117–124, Feb. 2012, doi: 10.1016/j.parkreldis.2011.07.014.

[10] M. G. Rizzone, M. Ferrarin, M. M. Lanotte, L. Lopiano, and I. Carpinella, "The dominant-subthalamic nucleus phenomenon in bilateral deep brain stimulation for Parkinson's disease: Evidence from a gait analysis study," *Frontiers Neurol.*, vol. 8, Oct. 2017, doi: 10.3389/fneur.2017.00575.

[11] D. Joshi, A. Khajuria, and P. Joshi, "An automatic non-invasive method for Parkinson's disease classification," *Comput. Methods Programs Biomed.*, vol. 145, pp. 135–145, Jul. 2017, doi: 10.1016/j.cmpb.2017.04.007.

[12] M. Ghislieri, M. Lanotte, M. Knaflitz, L. Rizzi, and V. Agostini, "Muscle synergies in Parkinson's disease before and after the deep brain stimulation of the bilateral subthalamic nucleus," *Sci. Rep.*, vol. 13, no. 1, pp. 1–13, Apr. 2023, doi: 10.1038/s41598-023-34151-6.

[13] J. W. Cohen, T. Vieira, T. D. Ivanova, G. L. Cerone, and S. J. Garland, "Maintenance of standing posture during multi-directional leaning demands the recruitment of task-specific motor units in the ankle plantarflexors," *Exp. Brain Res.*, vol. 239, no. 8, pp. 2569–2581, Aug. 2021, doi: 10.1007/s00221-021-06154-0.

[14] F. V. dos Anjos, M. Ghislieri, G. L. Cerone, T. P. Pinto, and M. Gazzoni, "Changes in the distribution of muscle activity when using a passive trunk exoskeleton depend on the type of working task: A high-density surface EMG study," *J. Biomechanics*, vol. 130, Jan. 2022, Art. no. 110846, doi: 10.1016/j.jbiomech.2021.110846.

[15] E. Anselmino, A. Mazzoni, and S. Micera, "EMG-based prediction of step direction for a better control of lower limb wearable devices," *Comput. Methods Programs Biomed.*, vol. 254, Sep. 2024, Art. no. 108305, doi: 10.1016/j.cmpb.2024.108305.

[16] C. Frigo and P. Crenna, "Multichannel SEMG in clinical gait analysis: A review and state-of-the-art," *Clin. Biomechanics*, vol. 24, pp. 236–245, Mar. 2009, doi: 10.1016/j.clinbiomech.2008.07.012.

[17] S. M. Keloth, R. Viswanathan, B. Jelfs, S. Arjunan, S. Raghav, and D. Kumar, "Which gait parameters and walking patterns show the significant differences between Parkinson's disease and healthy participants?" *Biosensors*, vol. 9, no. 2, p. 59, Apr. 2019, doi: 10.3390/bios9020059.

[18] A. Y. Meigal, S. M. Rissanen, M. P. Tarvainen, O. Airaksinen, M. Kankaanpää, and P. A. Karjalainen, "Non-linear EMG parameters for differential and early diagnostics (don't short) of Parkinson's disease," *Frontiers Neurol.*, vol. 4, p. 61099, Sep. 2013, doi: 10.3389/fneur.2013.00135.

[19] V. Agostini, M. Ghislieri, S. Rosati, G. Balestra, and M. Knaflitz, "Surface electromyography applied to gait analysis: How to improve its impact in clinics?" *Frontiers Neurol.*, vol. 11, pp. 1–13, Sep. 2020, doi: 10.3389/fneur.2020.00994.

[20] I. Mileti et al., "Muscle synergies in Parkinson's disease," *Sensors*, vol. 20, no. 11, p. 3209, Jun. 2020, doi: 10.3390/s20113209.

[21] V. Ruonala, E. Pekkonen, O. Airaksinen, M. Kankaanpää, P. A. Karjalainen, and S. M. Rissanen, "Levodopa-induced changes in electromyographic patterns in patients with advanced Parkinson's disease," *Frontiers Neurol.*, vol. 9, p. 35, Feb. 2018, doi: 10.3389/fneur.2018.00035.

[22] D. Torricelli et al., "Muscle synergies in clinical practice: Theoretical and practical implications," in *Emerging Therapies in Neurorehabilitation II*, vol. 10, J. Pons, R. Raya, and J. González, Eds., Cham, Switzerland: Springer, 2015, doi: 10.1007/978-3-319-24901-8_10.

[23] J. N. Kerkman, A. Daffertshofer, L. L. Gollo, M. Breakspear, and T. W. Boonstra, "Network structure of the human musculoskeletal system shapes neural interactions on multiple time scales," *Sci. Adv.*, vol. 4, no. 6, pp. 497–524, Jun. 2018, doi: 10.1126/sciadv.aat0497.

[24] T. W. Boonstra, A. Daffertshofer, M. Roerdink, I. Flipse, K. Groenewoud, and P. J. Beek, "Bilateral motor unit synchronization of leg muscles during a simple dynamic balance task," *Eur. J. Neurosci.*, vol. 29, no. 3, pp. 613–622, Feb. 2009, doi: 10.1111/j.1460-9568.2008.06584.x.

[25] J. N. Kerkman, A. Bekius, T. W. Boonstra, A. Daffertshofer, and N. Dominici, "Muscle synergies and coherence networks reflect different modes of coordination during walking," *Frontiers Physiol.*, vol. 11, Jul. 2020, Art. no. 535096, doi: 10.3389/fphys.2020.00751.

[26] E. Bullmore and O. Sporns, "Complex brain networks: Graph theoretical analysis of structural and functional systems," *Nature Rev. Neurosci.*, vol. 10, no. 3, pp. 186–198, Mar. 2009, doi: 10.1038/nrn2575.

[27] G. S. Bajestani, M. Behrooz, A. G. Khani, M. Nouri-Baygi, and A. Mollaei, "Diagnosis of autism spectrum disorder based on complex network features," *Comput. Methods Programs Biomed.*, vol. 177, pp. 277–283, Aug. 2019, doi: 10.1016/j.cmpb.2019.06.006.

[28] M. Rubinov and O. Sporns, "Complex network measures of brain connectivity: Uses and interpretations," *NeuroImage*, vol. 52, no. 3, pp. 1059–1069, Sep. 2010, doi: 10.1016/j.neuroimage.2009.10.003.

[29] S. G. Kobourov, "Spring embedders and force directed graph drawing algorithms," 2012, *arXiv:1201.3011*.

[30] R. Kenville et al., "Intermuscular coherence between homologous muscles during dynamic and static movement periods of bipedal squatting," *J. Neurophysiology*, vol. 124, no. 4, pp. 1045–1055, Oct. 2020, doi: 10.1152/jn.00231.2020.

[31] J. Gross et al., "The neural basis of intermittent motor control in humans," *Proc. Nat. Acad. Sci. USA*, vol. 99, no. 4, pp. 2299–2302, Feb. 2002, doi: 10.1073/pnas.032682099.

[32] F. Hug, A. Del Vecchio, S. Avrillon, D. Farina, and K. Tucker, "Muscles from the same muscle group do not necessarily share common drive: Evidence from the human triceps surae," *J. Appl. Physiol.*, vol. 130, no. 2, pp. 342–354, Feb. 2021, doi: 10.1152/japplphysiol.00635.2020.

[33] J. Levine, S. Avrillon, D. Farina, F. Hug, and J. L. Pons, "Two motor neuron synergies, invariant across ankle joint angles, activate the triceps surae during plantarflexion," *J. Physiol.*, vol. 601, no. 19, pp. 4337–4354, Oct. 2023, doi: 10.1113/jp284503.

[34] E. H. F. van Asseldonk, S. F. Campfens, S. J. F. Verwer, M. J. A. M. van Putten, and D. F. Stegeman, "Reliability and agreement of intramuscular coherence in tibialis anterior muscle," *PLoS ONE*, vol. 9, no. 2, Feb. 2014, Art. no. e88428, doi: 10.1371/journal.pone.0088428.

[35] T. W. Boonstra, "The potential of corticomuscular and intermuscular coherence for research on human motor control," *Frontiers Human Neurosci.*, vol. 7, pp. 1–2, Dec. 2013, doi: 10.3389/fnhum.2013.00855.

[36] T. W. Boonstra and M. Breakspear, "Neural mechanisms of intermuscular coherence: Implications for the rectification of surface electromyography," *J. Neurophysiology*, vol. 107, no. 3, pp. 796–807, Feb. 2012, doi: 10.1152/jn.00066.2011.

[37] C. M. Laine and F. J. Valero-Cuevas, "Intermuscular coherence reflects functional coordination," *J. Neurophysiology*, vol. 118, no. 3, pp. 1775–1783, Sep. 2017, doi: 10.1152/jn.00204.2017.

[38] M. Houston, X. Li, P. Zhou, S. Li, J. Roh, and Y. Zhang, "Alterations in muscle networks in the upper extremity of chronic stroke survivors," *IEEE Trans. Neural Syst. Rehabil. Eng.*, vol. 29, pp. 1026–1034, 2021, doi: 10.1109/TNSRE.2021.3075907.

[39] P. C. R. dos Santos, C. J. C. Lamoth, F. A. Barbieri, I. Zijdewind, L. T. B. Gobbi, and T. Hortobágyi, "Age-specific modulation of intermuscular beta coherence during gait before and after experimentally induced fatigue," *Sci. Rep.*, vol. 10, no. 1, pp. 1–12, Sep. 2020, doi: 10.1038/s41598-020-72839-1.

[40] T. Liang, H. Miao, H. Wang, X. Liu, and X. Liu, "Surface electromyography-based analysis of the lower limb muscle network and muscle synergies at various gait speeds," *IEEE Trans. Neural Syst. Rehabil. Eng.*, vol. 31, pp. 1230–1237, 2023.

[41] F. Faul, E. Erdfelder, A. Buchner, and A.-G. Lang, "Statistical power analyses using G*Power 3.1: Tests for correlation and regression analyses," *Behav. Res. Methods*, vol. 41, no. 4, pp. 1149–1160, Nov. 2009, doi: 10.3758/brm.41.4.1149.

[42] M. Ghislieri et al., "Improved dual-task interference in Parkinson's disease following deep brain stimulation," *IEEE Trans. Neural Syst. Rehabil. Eng.*, vol. 33, pp. 4624–4635, 2025, doi: 10.1109/TNSRE.2025.3632674.

[43] M. F. Folstein, S. E. Folstein, and P. R. McHugh, "'Mini-mental state': A practical method for grading the cognitive state of patients for the clinician," *J. Psychiatric Res.*, vol. 12, no. 3, pp. 189–198, Nov. 1975, doi: 10.1016/0022-3956(75)90026-6.

[44] B. Dubois, A. Slachevsky, I. Litvan, and B. Pillon, "The FAB: A frontal assessment battery at bedside," *Neurology*, vol. 55, no. 11, pp. 1621–1626, Dec. 2000, doi: 10.1212/wnl.55.11.1621.

[45] M. M. Hoehn and M. D. Yahr, "Parkinsonism: Onset, progression and mortality," *Neurology*, vol. 17, no. 5, pp. 427–442, 1967.

[46] C. G. Goetz et al., "Movement disorder society-sponsored revision of the unified Parkinson's disease rating scale (MDS-UPDRS): Process, format, and clinimetric testing plan," *Movement Disorders*, vol. 22, no. 1, pp. 41–47, Jan. 2007, doi: 10.1002/mds.21198.

[47] C. J. De Luca, L. Donald Gilmore, M. Kuznetsov, and S. H. Roy, "Filtering the surface EMG signal: Movement artifact and baseline noise contamination," *J. Biomechanics*, vol. 43, no. 8, pp. 1573–1579, May 2010, doi: 10.1016/j.jbiomech.2010.01.027.

[48] S. D. Nandedkar, C. Sheridan, S. Bertoni, B. C. Hiner, and P. E. Barkhaus, "Deep brain stimulator artifact in needle electromyography: Effects and distribution in paraspinal and upper limb muscle," *Muscle Nerve*, vol. 47, no. 4, pp. 561–565, Apr. 2013, doi: 10.1002/mus.23636.

[49] D. Glories, M. Soulhol, D. Amarantini, and J. Duclay, "Combined effect of contraction type and intensity on corticomuscular coherence during isokinetic plantar flexions," *Eur. J. Appl. Physiol.*, vol. 123, no. 3, pp. 609–621, Nov. 2023, doi: 10.1007/s00421-022-05087-y.

[50] Y. Ruiz-Gonzalez, L. Velázquez-Pérez, R. Rodríguez-Labrada, R. Torres-Vega, and U. Ziemann, "EMG rectification is detrimental for identifying abnormalities in corticomuscular and intermuscular coherence in spinocerebellar ataxia type 2," *Cerebellum*, vol. 19, no. 5, pp. 665–671, Oct. 2020, doi: 10.1007/s12311-020-01149-z.

[51] C. De Marchis, G. Severini, A. M. Castronovo, M. Schmid, and S. Conforto, "Intermuscular coherence contributions in synergistic muscles during pedaling," *Exp. Brain Res.*, vol. 233, no. 6, pp. 1907–1919, Jun. 2015, doi: 10.1007/s00221-015-4262-4.

[52] O. P. Neto and E. A. Christou, "Rectification of the EMG signal impairs the identification of oscillatory input to the muscle," *J. Neurophysiology*, vol. 103, no. 2, pp. 1093–1103, Feb. 2010, doi: 10.1152/jn.00792.2009.

[53] C. M. Laine and F. J. Valero-Cuevas, "Parkinson's disease exhibits amplified intermuscular coherence during dynamic voluntary action," *Frontiers Neurol.*, vol. 11, Apr. 2020, Art. no. 496079, doi: 10.3389/fneur.2020.00204.

[54] K. Zhao, Y. Feng, L. Li, Y. Zhou, Z. Zhang, and J. Li, "Muscle synergies and muscle networks in multiple frequency components in post-stroke patients," *Biomed. Signal Process. Control*, vol. 95, Sep. 2024, Art. no. 106417, doi: 10.1016/j.bspc.2024.106417.

[55] S. A. J. E. A. Lagerweij et al., "Intermuscular coherence as a biomarker of subthalamic nucleus deep brain stimulation efficacy in Parkinson's disease," *Clin. Neurophysiol.*, vol. 142, pp. 36–43, Oct. 2022, doi: 10.1016/j.clinph.2022.07.489.

[56] M. Mohr, M. Nann, V. von Tscharner, B. Eskofier, and B. M. Nigg, "Task-dependent intermuscular motor unit synchronization between medial and lateral vastii muscles during dynamic and isometric squats," *PLoS ONE*, vol. 10, no. 11, Nov. 2015, Art. no. e0142048, doi: 10.1371/journal.pone.0142048.

[57] M. W. Flood, B. R. Jensen, A.-S. Malling, and M. M. Lowery, "Increased EMG intermuscular coherence and reduced signal complexity in Parkinson's disease," *Clin. Neurophysiol.*, vol. 130, no. 2, pp. 259–269, Feb. 2019, doi: 10.1016/j.clinph.2018.10.023.

[58] J. B. Weersink, B. M. de Jong, and N. M. Maurits, "Neural coupling between upper and lower limb muscles in Parkinsonian gait," *Clin. Neurophysiol.*, vol. 134, pp. 65–72, Feb. 2022, doi: 10.1016/j.clinph.2021.11.072.

[59] L. Roeder, T. W. Boonstra, and G. K. Kerr, "Corticomuscular control of walking in older people and people with Parkinson's disease," *Sci. Rep.*, vol. 10, no. 1, pp. 1–18, Dec. 2020, doi: 10.1038/S41598-020-59810-W.

[60] T. H. Petersen, M. Kliim-Due, S. F. Farmer, and J. B. Nielsen, "Childhood development of common drive to a human leg muscle during ankle dorsiflexion and gait," *J. Physiol.*, vol. 588, no. 22, pp. 4387–4400, Nov. 2010, doi: 10.1113/jphysiol.2010.195735.

[61] C. E. Kerr, U. Agrawal, and S. Nayak, "The effects of tai chi practice on intermuscular beta coherence and the rubber hand illusion," *Frontiers Human Neurosci.*, vol. 10, p. 37, Feb. 2016, doi: 10.3389/fnhum.2016.00037.

[62] Z. Guo et al., "Altered corticomuscular coherence (CMCoh) pattern in the upper limb during finger movements after stroke," *Frontiers Neurol.*, vol. 11, May 2020, doi: 10.3389/fneur.2020.00410.

[63] A. N. Johnson and M. Shinohara, "Corticomuscular coherence with and without additional task in the elderly," *J. Appl. Physiol.*, vol. 112, no. 6, pp. 970–981, Mar. 2012, doi: 10.1152/japplphysiol.01079.2011.

[64] K. Terry and L. Griffin, "How computational technique and spike train properties affect coherence detection," *J. Neurosci. Methods*, vol. 168, no. 1, pp. 212–223, Feb. 2008, doi: 10.1016/j.jneumeth.2007.09.014.

[65] T. M. J. Fruchterman and E. M. Reingold, "Graph drawing by force-directed placement," *Softw., Pract. Exper.*, vol. 21, no. 1, pp. 1129–1164, Nov. 1991.

[66] P. Gajdoš, T. Ježowicz, V. Uher, and P. Dohnálek, "A parallel Fruchterman–Reingold algorithm optimized for fast visualization of large graphs and swarms of data," *Swarm Evol. Comput.*, vol. 26, pp. 56–63, Feb. 2016, doi: 10.1016/j.swevo.2015.07.006.

[67] V. D. Blondel, J.-L. Guillaume, R. Lambiotte, and E. Lefebvre, "Fast unfolding of communities in large networks," *J. Stat. Mechanics: Theory Exp.*, vol. 2008, no. 10, Oct. 2008, Art. no. P10008, doi: 10.1088/1742-5468/2008/10/p10008.

[68] M. E. J. Newman, "Analysis of weighted networks," *Phys. Rev. E, Stat. Phys. Plasmas Fluids Relat. Interdiscip. Top.*, vol. 70, no. 5, p. 9, Nov. 2004, doi: 10.1103/physreve.70.056131.

[69] F. Hug, S. Avrillon, A. Sarcher, A. Del Vecchio, and D. Farina, "Correlation networks of spinal motor neurons that innervate lower limb muscles during a multi-joint isometric task," *J. Physiol.*, vol. 601, no. 15, pp. 3201–3219, 2022.

[70] A. Lancichinetti and S. Fortunato, "Consensus clustering in complex networks," *Sci. Rep.*, vol. 2, no. 1, pp. 1–7, Mar. 2012, doi: 10.1038/srep00336.

[71] L. G. S. Jeub, O. Sporns, and S. Fortunato, "Multiresolution consensus clustering in networks," *Sci. Rep.*, vol. 8, no. 1, pp. 1–16, Feb. 2018, doi: 10.1038/s41598-018-21352-7.

[72] D. Jiménez-Grande, S. F. Atashzar, E. Martinez-Valdes, and D. Falla, "Muscle network topology analysis for the classification of chronic neck pain based on EMG biomarkers extracted during walking," *PLoS ONE*, vol. 16, no. 6, Jun. 2021, Art. no. e0252657, doi: 10.1371/journal.pone.0252657.

[73] J.-P. Onnela, J. Saramäki, J. Kertész, and K. Kaski, "Intensity and coherence of motifs in weighted complex networks," *Phys. Rev. E, Stat. Phys. Plasmas Fluids Relat. Interdiscip. Top.*, vol. 71, no. 6, p. 6, Jun. 2005, doi: 10.1103/physreve.71.065103.

[74] L. V. Hedges, "Distribution theory for glass's estimator of effect size and related estimators," *J. Educ. Statist.*, vol. 6, no. 2, pp. 107–128, Jun. 1981, doi: 10.3102/10769986006002107.

[75] A. Islam, L. Alcock, K. Nazarpour, L. Rochester, and A. Pantall, "Effect of Parkinson's disease and two therapeutic interventions on muscle activity during walking: A systematic review," *NPJ Parkinson's Disease*, vol. 1, no. 1, pp. 1–16, Sep. 2020, doi: 10.1038/s41531-020-00119-w.

[76] T. W. Boonstra, A. Danna-Dos-Santos, H.-B. Xie, M. Roerdink, J. F. Stins, and M. Breakspear, "Muscle networks: Connectivity analysis of EMG activity during postural control," *Sci. Rep.*, vol. 5, no. 1, pp. 1–14, Dec. 2015, doi: 10.1038/srep17830.

[77] P. Jensen et al., "Using corticomuscular and intermuscular coherence to assess cortical contribution to ankle plantar flexor activity during gait," *J. Motor Behav.*, vol. 51, no. 6, pp. 668–680, Nov. 2019, doi: 10.1080/00222895.2018.1563762.

[78] Q. Xiong et al., "Reduced corticospinal drive to antagonist muscles of upper and lower limbs during hands-and-knees crawling in infants with cerebral palsy: Evidence from intermuscular EMG-EMG coherence," *Behavioural Brain Res.*, vol. 457, Feb. 2024, Art. no. 114718, doi: 10.1016/j.bbr.2023.114718.

[79] A. A. da Silva Costa et al., "Corticomuscular and intermuscular coherence as a function of age and walking balance difficulty," *Neurobiol. Aging*, vol. 141, pp. 85–101, Sep. 2024, doi: 10.1016/j.neurobiolaging.2024.05.004.

[80] P. C. R. D. Santos, B. Heimler, O. Koren, T. Flash, and M. Plotnik, "Dopamine improves defective cortical and muscular connectivity during bilateral control of gait in Parkinson's disease," *Commun. Biol.*, vol. 7, no. 1, pp. 1–15, Apr. 2024, doi: 10.1038/s42003-024-06195-5.

[81] M. F. Rabbi, L. E. Diamond, C. P. Carty, D. G. Lloyd, G. Davico, and C. Pizzolato, "A muscle synergy-based method to estimate muscle activation patterns of children with cerebral palsy using data collected from typically developing children," *Sci. Rep.*, vol. 12, no. 1, p. 3599, Mar. 2022.

[82] L. Janshen, A. Santuz, A. Ekizos, and A. Arampatzis, "Fuzziness of muscle synergies in patients with multiple sclerosis indicates increased robustness of motor control during walking," *Sci. Rep.*, vol. 10, no. 1, pp. 1–14, Apr. 2020, doi: 10.1038/s41598-020-63788-w.

[83] X. Li, G. Xu, L. Li, Z. Hao, W. L. A. Lo, and C. Wang, "Analysis of muscle synergies and muscle network in sling exercise rehabilitation technique," *Comput. Biol. Med.*, vol. 183, Dec. 2024, Art. no. 109166, doi: 10.1016/j.compbiomed.2024.109166.

[84] M. Ghislieri, V. Agostini, and M. Knaflitz, "Muscle synergies extracted using principal activations: Improvement of robustness and interpretability," *IEEE Trans. Neural Syst. Rehabil. Eng.*, vol. 28, no. 2, pp. 453–460, Feb. 2020, doi: 10.1109/TNSRE.2020.2965179.

[85] D. Rimini, V. Agostini, and M. Knaflitz, "Intra-subject consistency during locomotion: Similarity in shared and subject-specific muscle synergies," *Frontiers Human Neurosci.*, vol. 11, pp. 1–10, Dec. 2017, doi: 10.3389/fnhum.2017.00586.

[86] C. J. De Luca, M. Kuznetsov, L. D. Gilmore, and S. H. Roy, "Inter-electrode spacing of surface EMG sensors: Reduction of crosstalk contamination during voluntary contractions," *J. Biomechanics*, vol. 45, no. 3, pp. 555–561, Feb. 2012, doi: 10.1016/j.jbiomech.2011.11.010.

[87] C. M. Germer, D. Farina, L. A. Elias, S. Nuccio, F. Hug, and A. Del Vecchio, "Surface EMG cross talk quantified at the motor unit population level for muscles of the hand, thigh, and calf," *J. Appl. Physiol.*, vol. 131, no. 2, pp. 808–820, Aug. 2021, doi: 10.1152/japplphysiol.01041.2020.

[88] S. Sveinbjornsdottir, "The clinical symptoms of Parkinson's disease," *J. Neurochemistry*, vol. 139, no. S1, pp. 318–324, Oct. 2016, doi: 10.1111/jnc.13691.